C. R. Mecanique 341 (2013) 386–392

Contents lists available at SciVerse ScienceDirect

Comptes Rendus Mecanique

www.sciencedirect.com

10th International Meeting on Thermodiffusion

Non-Fickian diffusion affects the relation between the salinity and hydrate capacity profiles in marine sediments

Denis S. Goldobin [a,b,*]

[a] Institute of Continuous Media Mechanics, UB RAS, 1 Acad. Korolev street, Perm 614013, Russia
[b] Department of Mathematics, University of Leicester, University Road, Leicester LE1 7RH, UK

ARTICLE INFO

Article history:
Available online 22 February 2013

Keywords:
Non-Fickian diffusion
Hydrate deposits
Brine salinity

ABSTRACT

On-site measurements of water salinity (which can be directly evaluated from the electrical conductivity) in deep-sea sediments is technically the primary source of indirect information on the capacity of the marine deposits of methane hydrates. We show the relation between the salinity (chlorinity) profile and the hydrate volume in pores to be significantly affected by non-Fickian contributions to the diffusion flux—the thermal diffusion and the gravitational segregation—which have been previously ignored in the literature on the subject and the analysis of surveys data. We provide amended relations and utilize them for an analysis of field measurements for a real hydrate deposit.

1. Introduction

Since being discovered methane hydrates have attracted significant attention. First estimates of their amount on the Earth, especially in the marine sediments, and their importance were extremely exaggerated. Today's assessment of their amount and role are more moderate and well underpinned by field data and results of numerical modelling and, thus, may be treated as realistic. Even with this "moderate" evaluation, research on natural hydrates in marine sediments is considered to be important.

In particular, methane hydrates present a potential hazard under anthropogenic climate change. The sensitivity of hydrate stability to changes in local pressure–temperature conditions and their existence beneath relatively shallow marine environments, mean that submarine hydrates are vulnerable to changes in bottom water conditions (e.g. warming). The potential climate impact of methane release following dissociation of hydrate in the past has been compared to climate feedbacks associated with the terrestrial biosphere and identified as a possible trigger of abrupt climate change (e.g., [1,2]). The role of hydrate disassociation as a trigger for submarine landslides has also been investigated [1,3,4], with reports of known hydrate occurrences that coincide with slumping and submarine landslides being common [4]. It is therefore imperative to improve our understanding of the global hydrate inventory. Studies [5,6] highlight that this improvement requires also certain revision of the physical and mathematical models of the marine deposits of methane hydrates employed in the literature [7–10].

Acquiring samples with methane hydrates from sediments beneath deep water bodies is a costly procedure which is not practically employed for large scale surveys [11]. Instead, the presence of hydrate is typically inferred from seismic data (e.g., [12]) or on-site salinity measurements in boreholes (e.g., [7]). The seismic data are (i) the presence of the "bottom-simulating reflector" which appears when hydrate deposit touches the bottom boundary of the hydrate stability zone and, therefore, is underlain by a free gas horizon [11,7,10] (Fig. 1), and (ii) sound speed increases in sediments with hydrates

* Corresponding author at: Department of Mathematics, University of Leicester, University Road, Leicester LE1 7RH, UK.
E-mail address: Denis.Goldobin@gmail.com.

1631-0721/$ – see front matter
http://dx.doi.org/10.1016/j.crme.2013.01.014

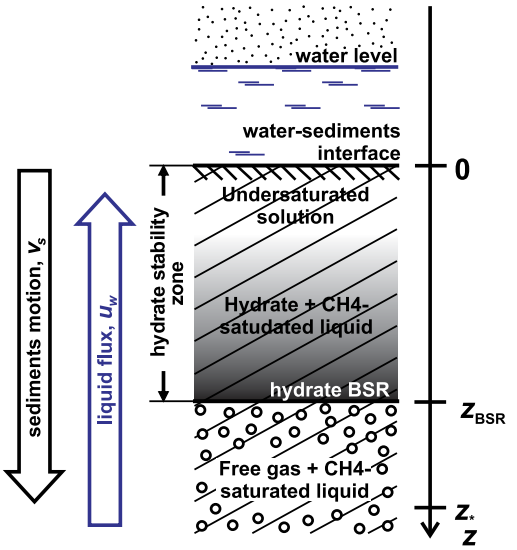

Fig. 1. (Color online.) Sketch of the marine sediments hosting a hydrate deposit with a free gas zone (*or* "bubble horizon") beneath the zone of the thermodynamic stability of methane hydrate. The boundary between the hydrate deposit and the free gas zone forms the bottom simulating reflector (BSR) of acoustic waves and can be seismically detected.

owing to the sediments cementation by hydrate in pores [12]. Both seismic techniques have significant limitations. For instance, the bottom simulating reflector appears only when hydrate deposit reaches the bottom edge of the hydrate stability zone, and the velocity increase owing to the sediment cementation does not allow accurate estimation of the amount of hydrate. Hence, on-site salinity measurements become an important source of information.

To date, the mathematical models reconstructing hydrate deposit parameters by means of fitting the measured salinity profiles disregard non-Fickian contributions to the diffusion flux of salt in sediments. In the present paper we (i) derive relations between the profiles of the hydrate volumetric fraction in pores and the measured salinity and (ii) demonstrate the non-Fickian contributions to be important.

The paper is organized as follows. In Section 2 we describe the transport processes in carbon-rich marine sediments and derive the relation between the salinity (chlorinity) and hydrate profiles. In Section 3 this relation is employed for reconstruction of the hydrate profile for a real natural hydrate deposit in the Blake Ridge hydrate province. In the concluding section we discuss importance of the non-Fickian diffusion and implementation of our reconstruction procedure.

2. Marine sediments hosting hydrate deposits: Transport processes

Real geological systems are much more uniform along two directions (say horizontal) than along the third direction (say vertical). Hence, we consider a one-dimensional problem with vertical spatial coordinate z (Fig. 1). On the field scale, such systems are featured by the temperature growth with depth:

$$T = T_{\mathrm{sf}} + Gz \tag{1}$$

where T_{sf} is the temperature of the water–sediment interface (*or* seafloor) and G is the geothermal gradient.

Methane is generated from the sediments by anaerobic bacteria. If the temperature is low enough and the pressure is high enough, methane forms hydrate. However, the critical pressure for the thermodynamic stability of hydrate depends on temperature nearly exponentially, and the hydrostatic pressure, which grows linearly with depth, cannot compensate the linear growth of temperature $T = T_{\mathrm{sf}} + Gz$ below a certain depth z_{BSR}. This depth z_{BSR} is the bottom boundary of the hydrate deposit: below this depth, hydrate is dissociated into water and methane-gas bubbles (Fig. 1).

The major part of natural hydrates of hydrocarbons on the Earth is a structure I clathrate of methane ($> 99\%$). The elementary cell of an "ideal" structure I clathrate is formed by 8 molecules of CH_4 and 46 molecules of H_2O, i.e., the mass fraction of water in the clathrate $K_{H_2O} = 23 \cdot 18/(23 \cdot 18 + 4 \cdot 16) \approx 0.866$. For real hydrates, the saturation of the structure with methane molecules is slightly less than 100%—some clathrate cages are not occupied by the methane molecule. In geological systems, the occupancy does not necessarily correspond to the thermodynamic equilibrium, because the hydrate was initially formed under the thermodynamic conditions of the place from where the hydrate was transported due to diverse geological processes. The relaxation rate of the occupancy is determined by the molecular diffusion of the methane molecules in hydrate clathrate (a solid matter) and is commensurable with rates of geological transport processes (100–1000 kyr). On the one hand, the actual local occupancy cannot be exactly evaluated from thermodynamical principles and the equilibrium condition, while, on the other hand, it is always higher than 95% [13], i.e. very close to the ideal value, 100%. Hence, we assume the "ideal" structure of hydrate, $K_{H_2O} \approx 0.866$.

Hydrate forming in pores consumes water from the brine while salts remains in the brine. Therefore, salt concentration increases and diffusion drives redistribution of the salt mass. This process determines the formation of the salinity (chlorinity) profile.

Additionally, one should distinguish the on-site chlorinity, ω_s, and the measured chlorinity, $\tilde{\omega}_s$, because the drilling procedure results in dissociation of hydrate and the release of the hydrate water into the brine at the measurement site [11]. Given the volumetric fraction of hydrate in pores is $h(z)$, the mass of NaCl in the unit volume of pores before the dissociation of hydrate, $\omega_s\rho_w(1-h)$, equals the mass after dissociation, $\tilde{\omega}_s(\rho_w(1-h)+K_{H_2O}\rho_h h)$, where $\rho_w = 1000$ kg/m^3 is the water density, $\rho_h = 930$ kg/m^3 is the hydrate density. Hence,

$$\tilde{\omega}_s = \omega_s\left(1-\frac{K_{H_2O}\rho_h}{\rho_w}h+\mathcal{O}\left(\left(1-\frac{K_{H_2O}\rho_h}{\rho_w}\right)^2 h^2\right)\right)\approx\omega_s\left(1-\frac{K_{H_2O}\rho_h}{\rho_w}h\right)\equiv\omega_s(1-kh) \tag{2}$$

where

$$k\equiv\frac{K_{H_2O}\rho_h}{\rho_w}\approx 0.805$$

the correction $\mathcal{O}[(1-k)^2h^2]=\mathcal{O}[(0.03\cdot h)\cdot h]$ for real systems, where h rarely exceeds 7% [7,10], is less than $0.002\cdot h$ and can be neglected.

Since the salt is transported with pore water, we have to describe the water mass transport in the system. The water mass is transported as a part of hydrate, with sediments, and with the brine, by the pore water flux. The downward transport of sediments is significantly affected by the sediments compaction with depth [7,11]; the porosity ϕ significantly decreases with depth according to the empiric law:

$$\phi(z)=\phi_0\exp(-z/L) \tag{3}$$

where L is the depth of e-folding of porosity. The mass conservation law for sediments yields:

$$v_s(z)=\frac{1-\phi_0}{1-\phi(z)}v_{s0} \tag{4}$$

where $v_s(z)$ is the sediment motion velocity. This relation is nearly not affected by the conversion of part of sediments into methane. Indeed, the defect of the solid matrix volume owing to methane generation is approximately $\Delta V_s=\Delta m_{CH_4}/\rho_s$ ($\rho_s\approx 2650$ kg/m^3 is the sediment material density [7]), whereas the production of hydrate ΔV_h from this mass of methane is $\Delta m_{CH_4}/K_{H_2O}\rho_h$. The ratio $\Delta V_s/\Delta V_h = K_{H_2O}\rho_h/\rho_s\approx 0.04$ is small and thus ΔV_s, related to methane generation, is negligible.

For water, the mass conservation law reads:

$$\frac{\partial}{\partial t}\left(\phi(1-h-b)\rho_w+\phi h K_{H_2O}\rho_h\right)=-\frac{\partial}{\partial z}(\rho_w u_w)-\frac{\partial}{\partial z}(\phi h K_{H_2O}\rho_h v_s) \tag{5}$$

where b is the volumetric fraction of bubbles in the pore volume ($h=0$ beyond the hydrate stability zone, $b=0$ within it), u_w is the brine filtration velocity. Following Davie and Buffett [7,8], we consider a steady-state situation and set time derivatives to zero. Hence,

$$\rho_w u_w(z)+\phi(z)h(z)K_{H_2O}\rho_h v_s(z)=\rho_w u_w(0)$$

(hydrate is not present close to the water–sediment interface, $h(0)=0$), and, substituting $v_s(z)$ from Eq. (4), we find:

$$u_w = u_{w0}-k\phi h\frac{1-\phi_0}{1-\phi}v_{s0} \tag{6}$$

Given that the brine filtration velocity u_w is known (Eq. (6)), one can evaluate the salt transport from the mass conservation law;

$$\frac{\partial}{\partial t}\left(\phi(1-h-b)\rho_w\omega_s\right)=-\frac{\partial}{\partial z}(\rho_w\omega_s u_w)-\frac{\partial}{\partial z}J_{s,\mathrm{diff}} \tag{7}$$

The diffusive flux $J_{s,\mathrm{diff}}$ of the NaCl mass is contributed by the Fickian molecular diffusion flux and non-Fickian diffusion fluxes—the thermal diffusion and gravitational segregation (importance of which for the gas transport in geological systems under consideration was previously demonstrated [5]). The diffusive flux reads [14,5]:

$$J_{s,\mathrm{diff}}=-\chi\phi(1-h-b)D_s\rho_s\omega_s\left(\frac{\partial}{\partial z}\ln\omega_s+\alpha_s\frac{\partial}{\partial z}\ln T-\frac{\tilde{\mu}_s g}{RT}\right) \tag{8}$$

The following notations are introduced here:

- χ is the tortuosity factor, which characterizes the effect of the pore morphology on the effective diffusivity of species in pore fluid. For our system, $\chi = 0.75$ [15];

- D_s is the molecular diffusion coefficient in bulk brine;
- α_s is the thermodiffusion constant;
- $g = 9.8\ \mathrm{m/s^2}$ is the gravity;
- the universal gas constant $R = 8.314\ \mathrm{J/(mol\,K)}$;
- $\tilde{\mu}_s = \mu_{\mathrm{NaCl}} - N\mu_{\mathrm{H_2O}}$ is the effective molar mass of the pair of ions Na^+ and Cl^- in the aqueous solution, N is the number of water molecules in the volume occupied by this pair in the solvent, which can be evaluated from the dependence of the solution density on its concentration (see, e.g., Appendix A in [5]):

$$\tilde{\mu}_s = \frac{\mu_{\mathrm{NaCl}}}{\rho_w}\frac{\partial \rho_{\mathrm{solution}}}{\partial \omega_s}\bigg|_{\omega_s=0} \approx 42\ \mathrm{g/mol}$$

In [16], the thermodiffusion constant α_s and the molecular diffusion coefficient D_s were measured for a seminormal aqueous solution of NaCl. For the thermodiffusion constant, a sign inversion was observed near $T_i = 12\,^\circ\mathrm{C}$. In the temperature range typical for our system, $T \in (275\ \mathrm{K}, 305\ \mathrm{K})$, the temperature dependencies of α_s and D_s are strong and well represented by expressions:

$$\alpha_s \approx 0.0246\ \mathrm{K^{-1}}(T - T_i) \quad \text{and} \quad D_s \approx 6.1\cdot 10^{-10}\exp\left[0.0371\ \mathrm{K^{-1}}(T - 273.15\ \mathrm{K})\right]\mathrm{m^2/s}$$

Hydrostatic pressure in marine sediments, which is up to several hundreds atmospheres, is not strong enough to affect the diffusion constant of chemicals in water.

For a steady state, Eqs. (7) and (8) yield

$$\omega_s u_w - \chi\phi(1-h-b)D_s\omega_s\left(\frac{\partial}{\partial z}\ln\omega_s + \alpha_s\frac{\partial}{\partial z}\ln T - \frac{\tilde{\mu}_s g}{RT}\right) = \omega_{s*}u_{w*} + J_{s,\mathrm{diff}*} \tag{9}$$

where $\omega_{s*} \equiv \omega_s(z_*)$, $u_{w*} \equiv u_w(z_*) = u_{w0}$, $J_{s,\mathrm{diff}*} \equiv J_{s,\mathrm{diff}}(z_*)$, and z_* is a certain depth deep below the hydrate stability zone (see Fig. 1). Hereafter, the sign "$*$" indicates the value at depth z_*.

Since $h \ll 1$, we restrict our consideration to the linear in h (and b) approximation. Substituting Eqs. (2) and (6) into Eq. (9), we can find:

$$\frac{\partial h}{\partial z} + \gamma(z)h = f(z) \tag{10}$$

where

$$\gamma(z) = \frac{1}{\chi D_s}\left(\frac{1-\phi_0}{1-\phi}v_{s0} - \frac{u_{w0}}{\phi}\right)$$

$$f(z) = -\frac{1}{k}\left(\frac{1}{\tilde{\omega}_s}\frac{\partial\tilde{\omega}_s}{\partial z} + \beta\frac{G}{T}\right) + \frac{\phi_* D_{s*}}{k\phi D_s}\left(\frac{1}{\tilde{\omega}_{s*}}\frac{\partial\tilde{\omega}_{s*}}{\partial z} + \beta_*\frac{G_*}{T_*}\right) + \frac{u_{w0}}{k\chi\phi D_s}\left(1 - \frac{\tilde{\omega}_{s*}}{\tilde{\omega}_s}\right)$$

and the parameter

$$\beta \equiv \alpha_s(T) - \frac{\tilde{\mu}_s g}{RG}$$

characterizes the strength of the non-Fickian flux.

With Eq. (10), one can reconstruct the hydrate profile $h(z)$ from the measured chlorinity profile $\tilde{\omega}_s(z)$. Although one can write down an analytical solution to the problem (10):

$$h(z) = \int_0^z f(z_1)e^{-\int_{z_1}^z \gamma(z_2)\,\mathrm{d}z_2}\,\mathrm{d}z_1$$

numerical integration of Eq. (10) is more convenient for data analysis in practice. Remarkably, the relation between $h(z)$ and $\tilde{\omega}_s(z)$ does not involve quantitative data on the process and history of the formation of hydrate deposit and the process of generation of methane from sediments.

3. Salinity profile analysis and hydrate profile reconstruction

We demonstrate application of our results to the analysis of one of the most important marine hydrate provinces—the Blake Ridge. For the Ocean Drilling Program site 997, on the Blake Ridge, extensive data have been acquired, including hydrate samples and the on-site salinity (chlorinity) measurements [11] (Fig. 2(a)). The reported parameters for this site are presented in Table 1. We have two parameters which are not imposed by the results of direct measurements: sedimentation rate v_{s0} and filtration velocity u_{w0}.

In natural systems, the hydrate deposit cannot be in touch with the water–sediment interface, because aqueous methane concentration in the water body above the sediments is zero and hydrate must dissociate. Moreover, in seas, methane is

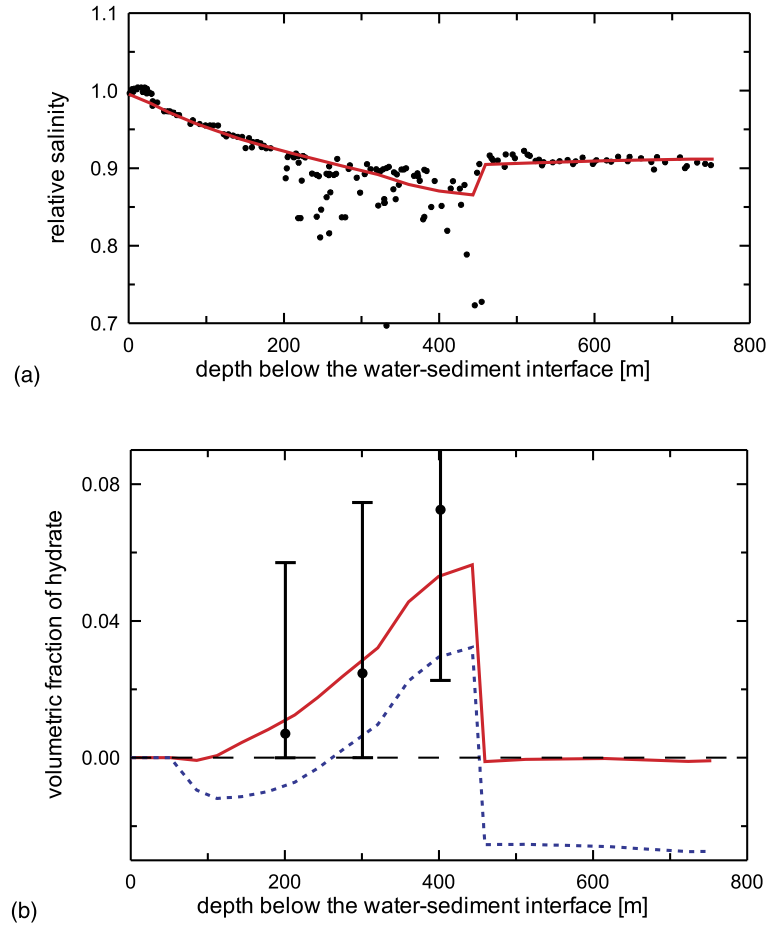

Fig. 2. (Color online.) (a): Measured chlorinity profile (solid circles) and smoothed chlorinity profile used for calculation of the hydrate profile (red solid line) for the site 997 of the Ocean Drilling Program [11]. (b): Hydrate profile reconstructed from the chlorinity data with Eq. (10) is plotted with the red solid line (parameters are specified in Table 1 and $u_{w0} = -8$ cm/kyr, $v_{s0} = 9$ cm/kyr). For demonstration, we plot a *formal* hydrate profile for purely Fickian diffusion flux of the same strength (blue dashed line). Non-Fickian contributions are obviously non-negligible. Indeed, the latter profile significantly deviates from the former one and possesses unphysical features: negative values of the hydrate volumetric fraction and non-zero (negative) amount of hydrate beyond the zone of the thermodynamic stability of hydrate. The black points with confidence intervals represent the values reconstructed from acoustic data [17].

Table 1
Geophysical properties for the Ocean Drilling Program site 997.

T_{sf}	water–sediment interface temperature, Eq. (1)	2 °C	Refs. [11,7]
G	geothermal gradient, Eq. (1)	35 °C/km	Refs. [11,7]
$\phi(0)$	seafloor porosity, Eq. (3)	0.69	Ref. [7]
L	e-folding depth of porosity, Eq. (3)	2 km	Ref. [7]

oxidized by sulfates, which are present in sea water, and its concentration is zero within the so-called sulfate reduction zone, which typically expands approximately 20 m below the water–sediment interface [8]. Hence, hydrate should not be present in a quiet extended upper part of the hydrate stability zone. With Eq. (10), the absence of hydrate, $h = 0$, requires $f(z) = 0$ next to $z = 0$. The function $f(z)$ is independent of v_{s0} and we can set it to zero for small z by tuning u_{w0}. With the chlorinity profile plotted in Fig. 2(a), this procedure yields $u_{w0} = -(8 \pm 0.5)$ cm/kyr (the flux is negative, i.e. ascending). One can see that for $u_{w0} = -8$ cm/kyr, $h = 0$ down to depths slightly over 100 m, while for different filtration velocity it deviates from zero next to $z = 0$ m. Furthermore, with fixed u_{w0}, the reconstructed amount of hydrate below the hydrate stability zone (for $z > 450$ m in Fig. 2) depends on v_{s0} monotonically; it vanishes for $v_{s0} = (9 \pm 0.5)$ cm/kyr (Fig. 2(b)). The hydrate profile plotted in Fig. 2(b) with the red solid line is the final result of the reconstruction of the hydrate profile from the measured chlorinity profile plotted in Fig. 2(a).

The amount of hydrate can be completely independently assessed from acoustic data [17]. In Fig. 2(b), the black points with confidence intervals represent the hydrate amount evaluated in [17] averaged over 100 m intervals. The estimates

of hydrate amount from acoustic data are typically featured by large uncertainty (notice broad confidence intervals); in Fig. 2(b), our evaluation of hydrate profile is in agreement with these estimates up to their accuracy.

It is noteworthy that our reconstruction procedure is free of uncertainties in parameters: all but two parameters are available from direct measurements and these two parameters are strictly imposed by two inevitable inherent features of the hydrate profile.

4. Conclusion and discussion

In this paper the transport of water and salt have been considered for marine sediments hosting natural hydrate deposits. The mathematical description employed accounts for

- non-Fickian diffusion of NaCl, and
- temperature dependence of the molecular diffusivity.

We have demonstrated the crucial importance of the both, whereas they are disregarded in the literature on the modelling of marine hydrate deposits (e.g., [7–10]). Based on this consideration, we have derived the relation between the measured salinity (chlorinity) profile and the hydrate profile. Application of this relation has been demonstrated for a real hydrate deposit (Fig. 2).

The solution, we found for this "reverse engineering" problem, does not involve quantitative data on the process and history of the formation of hydrate deposit and the process of generation of methane from sediments. This is an important feature of our results because presently, in the literature, closed models of hydrate formation involve particular assumptions on the generation process (e.g., [7,8]). In these studies the entire model is tested against the measured salinity profile, while we can see that only the current hydrate profile determines the salinity profile. Moreover, the sedimentation rate is unambiguously imposed by features of one of these profiles, whereas it has been previously indirectly inferred from geological data.

Importantly, our reconstruction procedure is free of uncertainties in model parameters: all but two parameters—sedimentation rate v_{s0} and filtration velocity u_{w0}—are available from direct measurements. These two parameters are strictly imposed by two inherent features of the hydrate profile: the absence of hydrate (i) close to the water–sediment interface and (ii) beneath the hydrate stability zone.

Acknowledgements

The work has been financially supported by the Government of Perm Region (Contract C-26/212) and Grant of The President of Russian Federation (MK-6932.2012.1).

References

[1] M. Maslin, et al., Gas hydrates: Past and future geohazard? Phil. Trans. R. Soc. A 368 (2010) 2369–2393.
[2] J. Maclennan, S.M. Jones, Regional uplift, gas hydrate dissociation and the origins of the Paleocene–Eocene Thermal Maximum, Earth Planet. Sci. Lett. 245 (2006) 65–80;
T. Dunkley Jones, et al., A palaeogene perspective on climate sensitivity and methane hydrate instability, Phil. Trans. R. Soc. A 368 (2010) 2395–2415;
J.P. Kennett, et al., Methane Hydrates in Quaternary Climate Change: The Clathrate Gun Hypothesis, AGU, Washington, DC, 2003;
E.G. Nisbet, The end of the ice age, Can. J. Earth Sci. 27 (1990) 148–157;
C.K. Paull, W. Ussler, W.P. Dillon, Is the extent of glaciation limited by marine gas hydrates? Geophys. Res. Lett. 18 (1991) 432–434.
[3] K.A. Kvenvolden, Potential effects of gas hydrate on human welfare, PNAS 96 (1999) 3420–3426;
R.D. McIver, Role of naturally occuring gas hydrates in sediment transport, Am. Assoc. Pet. Geol. Bull. 66 (1982) 789–792.
[4] J.-P. Henriet, J. Mienert, Gas hydrates: Relavance to world margin stability and climate change, Spec. Publ. Geol. Soc. Lond. 137 (1998);
T. Bugge, S. Befring, R.H. Belderson, A giant three-stage submarine slide off Norway, Geo-Mar. Lett. 7 (1987) 191–198;
R.E. Kayen, H.J. Lee, Pleistocene slope instability of gas hydrate-laden sediment on the Beaufort sea margin, Mar. Geotechnol. 10 (1991) 125–141.
[5] D.S. Goldobin, N.V. Brilliantov, Diffusive counter dispersion of mass in bubbly media, Phys. Rev. E 84 (2011) 056328;
D.S. Goldobin, et al., Non-Fickian diffusion and the accumulation of methane bubbles in deep-water sediments, arXiv:1011.6345.
[6] D.S. Goldobin, Scaling of transport coefficients of porous media under compaction, Europhys. Lett. 95 (2011) 64004.
[7] M.K. Davie, B.A. Buffett, A numerical model for the formation of gas hydrate below the seafloor, J. Geophys. Res. 106 (2001) 497–514.
[8] M.K. Davie, B.A. Buffett, A steady state model for marine hydrate formation: Constraints on methane supply from pore water sulfate profiles, J. Geophys. Res. 108 (2003) 2495.
[9] M.K. Davie, B.A. Buffett, Sources of methane for marine gas hydrate: Inferences from a comparison of observations and numerical models, Earth Planet. Sci. Lett. 206 (2003) 51–63.
[10] D. Archer, Methane hydrate stability and anthropogenic climate change, Biogeosciences 4 (2007) 521–544;
S.K. Garg, et al., A mathematical model for the formation and dissociation of methane hydrates in the marine environment, J. Geophys. Res. 113 (2008) B01201;
R.R. Haacke, G.K. Westbrook, M.S. Riley, Controls on the formation and stability of gas hydrate-related bottom-simulating reflectors (BSRs): A case study from the west Svalbard continental slope, J. Geophys. Res. 113 (2008) B05104.
[11] C.K. Paull, R. Matsumoto, P.J. Wallace, W.P. Dillon (Eds.), Proceedings of the Ocean Drilling Program, in: Scientific Results, vol. 164, Ocean Drilling Program, College Station, TX, 2000.
[12] C. Ecker, J. Dvorkin, A. Nur, Estimating the amount of hydrate and free gas from surface seismic, SEG Tech. Program Expanded Abstracts 17 (1998) 566–569.

[13] S. Circone, S.H. Kirby, L.A. Stern, Direct measurement of methane hydrate composition along the hydrate equilibrium boundary, J. Phys. Chem. B 109 (2005) 9468–9475.
[14] R.B. Bird, W.E. Stewart, E.N. Lightfoot, Transport Phenomena, 2nd ed., Wiley, 2007.
[15] F.A. Butt, A. Elverhoi, A. Solheim, C.F. Forsberg, Deciphering late lenozoic development of the western Svalbard margin from ODP 986 results, Mar. Geol. 169 (2000) 373–390.
[16] D.R. Caldwell, Thermal and Fickian diffusion of sodium chloride in a solution of oceanic concentration, Deep Sea Res. Oceanogr. Abstr. 20 (1973) 1029–1039;
D.R. Caldwell, Measurements of negative thermal diffusion coefficients observing onset of thermohaline convection, J. Phys. Chem. 77 (1973) 2004.
[17] M.W. Lee, Gas hydrates amount estimated from acoustic logs at the Blake Ridge, sites 994, 995, and 997, in: C.K. Paull, R. Matsumoto, P.J. Wallace, W.P. Dillon (Eds.), Proceedings of the Ocean Drilling Program, in: Scientific Results, vol. 164, Ocean Drilling Program, College Station, TX, 2000.